communications earth & environment

Article

A Nature Portfolio journal

https://doi.org/10.1038/s43247-025-02420-z

# Enhanced continental weathering drove a transient oxygenation event during the largest Ediacaran carbon isotope excursion

Check for updates

He Sun [1] ✉, Yilin Xiao [2,3] ✉, Yangyang Wang[2], Fengtai Tong[2,4], Hai-Ou Gu[1], Can Ge[1], Fangyue Wang[1,5], Zhihui An[6], Erhao Shan[2], Meng Zhang[2], Tingyu Yang[2] & Pengju Liu[7]

The largest Ediacaran carbon isotope excursion (the Shuram excursion, SE) has been proposed to coincide with a transient oceanic oxygenation event. However, the mechanisms responsible for the SE and the associated oxygenation remain unclear. In this study, we investigated the role of silicate weathering during the SE by measuring Li isotope compositions from two suites of marine carbonates in the Ediacaran Doushantuo sections. Our results reveal a pronounced negative lithium isotope excursion during the SE, which cannot be attributed to mineralogical effects and argues against a diagenetic origin for the SE. Instead, box model simulations of lithium-strontium cycles suggest a pulsed phase of enhanced congruent continental weathering during the SE. This increased weathering would have significantly elevated the input of essential nutrients into the ocean, boosting primary production, which in turn led to transient oceanic oxygenation. This process may also explain the negative $\delta^{13}C_{carb}$ excursion, as it could result from the oxidation of upwelling dissolved organic carbon in shallow seawater. Continental weathering likely played a crucial role in regulating climate, seawater chemistry, and Earth's surface oxidation state during the SE.

The late Ediacaran Period was a pivotal time in Earth's history, marked by the biological evolution of early metazoans around 574 − 541 Ma, commonly referred to as the "Ediacara biota"[1]. Concurrent with this event, extremely negative carbonate-carbon isotope ($\delta^{13}C_{carb}$) values were recorded in Ediacaran basins worldwide, known as the Shuram Excursion (SE)[2]. During the SE, $\delta^{13}C_{carb}$ dropped from +3‰ – −12‰ before gradually rising to ~+4‰ over ~7 million years (SE duration: ~574.0 ± 4.7 to 567.3 ± 3.0 Ma)[3], making it the largest negative inorganic carbon isotope excursion in Earth's history.

The mechanisms driving the SE remain debated, with hypotheses ranging from post-depositional diagenesis and global marine transgression to recycled carbonatite eruptions and the oxidation of dissolved organic carbon (DOC)[2,4–7]. The correlation between $\delta^{13}C_{carb}$ and $\delta^{18}O_{carb}$ values in carbonates has led to the suggestion that the SE could be a result of later diagenetic alteration, meaning it might not represent true seawater signatures[5,7]. However, the global nature of the SE, along with recent in-situ petrographic and high-resolution C-O and Ca isotope analyses, supports the idea that the SE signal primarily reflects seawater conditions with minimal alteration by meteoric fluids or late-stage diagenesis[6,8]. One widely proposed explanation for the SE involves deep ocean oxygenation, leading to the oxidation of $^{13}C$-depleted organic carbon reservoirs[9,10]. This mechanism seems conducive to the radiation of the Ediacaran biota. Although still debated[11,12], the oxygenation hypothesis has gained additional support from various geochemical proxies, including elemental (P, Mo concentrations, and iron speciation) and isotopic (S, U, Tl, and triple-oxygen) signatures in carbonate and shale formations[10,13–18], as well as organic redox proxies[19]. This oxygenation event appears transient (~7 Myr) and closely coincides with the SE[3]. Despite recent advances, the trigger and cause of the

[1]Hefei University of Technology, School of Resources and Environmental Engineering, Hefei, 230009, China. [2]State Key Laboratory of Lithospheric and Environmental Coevolution, School of Earth and Space Sciences, University of Science and Technology of China, Hefei, 230026, China. [3]CAS Center for Excellence in Comparative Planetology, Hefei, 230026, China. [4]International Center for Isotope Effects Research School of Earth Sciences and Engineering, Nanjing University, Nanjing, 210023, PR China. [5]Anhui Provincial Key Laboratory for Deep Exploration, Evaluation and Utilization of Strategic Mineral Resources, Hefei, 230009 Anhui, People's Republic of China. [6]Hubei Key Laboratory of Paleontology and Geological Environment Evolution, Wuhan Center of China Geological Survey, Wuhan, 430205, China. [7]Institute of Geology, Chinese Academy of Geological Sciences, Beijing, 10037, China. ✉e-mail: sunhe@hfut.edu.cn; ylxiao@ustc.edu.cn

oxygenation event, the source of the oxidants, and the extent of oceanic oxygenation during the SE remain subjects of ongoing debate[5,11,13,18]. It has been suggested that increased weathering inputs of sulfide and nutrients, such as phosphorus (P), drove extensive sulfur oxidation and boosted primary production in the SE ocean. This process may have invoked further P release during marine organic matter oxidation, leading to P-O cycling distinct from that in modern oceans[20]. Understanding whether enhanced continental weathering occurred simultaneously is crucial for unraveling the origin of the SE, yet direct evidence supporting such weathering has been lacking. The primary geochemical evidence suggesting enhanced weathering during the SE comes from the seawater $^{87}Sr/^{86}Sr$ record, which shows an increase from <0.708 to ~0.709[21]. However, $^{87}Sr/^{86}Sr$ is not a straightforward proxy for continental weathering, as it is influenced not only by riverine input from continental weathering (more radiogenic) and mantle input from mid-ocean ridges and seafloor (less radiogenic), but also by the weathering of different lithologies, such as basalt and granite.

The lithium (Li) isotopic composition of seawater ($\delta^7Li_{SW}$), primarily reconstructed from marine biogenic or abiogenic bulk carbonates, has proven to be a valuable tracer for continental weathering[22–28]. As one of the main sources of Li in seawater, the riverine flux of Li and its isotopic composition is crucial for linking continental silicate weathering to variations in seawater Li isotopes[24]. The dissolved Li flux is positively correlated with the denudation rate[25]. Dissolved $\delta^7Li$ in global rivers generally exhibit a negative correlation with weathering intensity and Li concentrations ([Li]). Elevated riverine $\delta^7Li$ values (up to 42‰) correspond to intermediate to high silicate weathering intensity and moderate [Li] levels (0.01 to 0.2 μM), occurring under incongruent weathering regimes where secondary clay minerals form abundantly. In contrast, low riverine $\delta^7Li$ values (approaching continental crust values of 0-4‰) are associated with congruent weathering regimes. These may reflect either high silicate weathering intensity with low [Li] or extremely low chemical weathering intensity combined with intense physical erosion, resulting in high [Li] levels of up to ~1 to 10 μM[25]. By applying static or dynamic box models of seawater[23,24,26,28,29] and incorporating past seafloor spreading rates to estimate hydrothermal and subduction reflux fluxes, riverine Li input can be constrained using reconstructed $\delta^7Li_{SW}$. This provides a foundation for using marine bulk carbonate $\delta^7Li$ to trace past continental silicate weathering[23,24,26,28].

In this study, we use Li isotopes as a proxy for continental weathering, providing direct geochemical evidence of a pulse of enhanced congruent continental weathering coincident with the SE. This enhanced weathering likely increased the influx of essential nutrients, such as P, Fe, and Ca, into the ocean, boosting primary production, or transporting oxidants like sulfate directly into marine environments[13]. These processes could have contributed to the rise of $O_2$ in the ocean and atmosphere, as well as the SE, through the oxidation of upwelling DOC in shallow seawater.

## Results

Our Li isotope analyses focus on marine carbonates collected from the CJYZ and JLW sections, two profiles of the Ediacaran Doushantuo Formation that recorded the SE in the Three Gorges area, South China[30] (Fig. 1). The data presented here reveal a pronounced Li isotope excursion across the SE (Fig. 2). In the CJYZ bulk carbonates, $\delta^7Li_{carb}$ declines from ~+16.5 ± 5.7‰ to ~+7.5‰, followed by an increase to +14.7‰, which correlates well with $\delta^{13}C_{carb}$ signals. Samples leached in both 0.3 M and 0.5 M acetic acid exhibit consistent trends in $\delta^7Li$ and elemental ratios (Fig. 2a), validating the reproducibility of the data. However, the Li isotopic excursion in the CJYZ section is incomplete due to the absence of carbonate deposition during the peak of the SE.

The JLW section displays similar patterns, with $\delta^7Li_{carb}$ dropping from ~ +14.1 ± 3.8‰ to ~ +6.6 ± 3.9‰, followed by an increase to ~ +17.2 ± 3.0‰. This distinct Li isotope excursion recorded in bulk marine carbonates also coincides broadly with the increases in seawater Sr isotopes[31]. The Li/(Ca+Mg) ratio remains consistently lower at 5.9 ± 6.7 μmol/mol during the SE, compared to the pre-SE (13.1 ± 9.7 μmol/mol) and the end-SE period (16.5 ± 13.5 μmol/mol) in the JLW section. Meanwhile, Sr/(Ca+Mg) exhibits a "W-shaped" pattern across the section, with a decreasing trend in the pre-SE strata, a rebound at the onset of SE (~0.1 mmol/mol) to the mid-SE (0.3 mmol/mol), and a subsequent decline to ~0.15 mmol/mol toward the end of the SE, followed by a rapid increase end-SE (Fig. 2). High Sr/Ca ratios observed in the mid-SE are consistent with findings from SE sections in China, Australia, the USA, Canada, Oman, and Peru[6,21], suggesting that these secular changes in Sr/(Ca+Mg) may represent a global trend during the SE.

### Evaluations of clay contaminations

Clay minerals contain significantly higher Li concentrations and much lighter $\delta^7Li$ values than carbonate minerals, meaning even a small degree of clay contamination could lower the Li isotopic composition of acetic-acid leachate[27]. Since the concentrations of Al, Li, and Sr differ substantially between clay and carbonate minerals, we used these elements to assess the extent of clay contamination. The Al/(Mg+Ca) molar ratios of the samples range from 0.03 to 0.55 mmol/mol (average 0.24 mmol/mol) for the CJYZ section and 0.03 to 0.93 mmol/mol (average 0.30 mmol/mol) for the JLW section—values that are significantly lower than those found in aluminosilicate rocks (~4780 mmol/mol for post-Archean average shale, and ~35300 mmol/mol for Low-Calcic Shales)[32], suggesting little clay mineral contamination (<0.02%).

To further screen for potential clay contamination, conservative thresholds of Li/(Mg + Ca)> 40 μmol/mol, Al/(Mg + Ca)> 0.64 mmol/mol, and Al/Sr > 6 mol/mol were applied here to screen for possible clay contamination (Supplementary Fig. 1). A total of 13 out of 179 samples have been screened, and the trend of Li isotopes persists. No negative correlation is observed between $\delta^7Li$ and element ratios of Li/(Mg+Ca), Al/(Mg+Ca), and Al/Sr. The samples with relatively low $\delta^7Li$ often exhibit low Li/(Mg+Ca) and Al/Sr values (Supplementary Fig. 1b, c). These observations strongly argue against clay mineral control of the Li isotopic variations in the acetic-acid leachate. Therefore, we consider the Li isotopic variations of acetic-acid leachate faithfully reflecting the signal of carbonates.

### Evaluations of mineralogical effects

The two studied profiles exhibit different sedimentary sequences across the SE[30,33]. The CJYZ section consists mainly of dolostones in the pre-SE and terminal of SE, with a 20 meter-thick black shale unit deposited during the peak of the SE. As a result, the CJYZ section recorded an incomplete negative Li isotopic excursion in the dolostones, with a data gap corresponding to the black shale deposition during the climax of the SE (Fig. 2a). In contrast, the JLW section has a more complete carbonate record across the SE, capturing a detailed Li isotopic excursion (Fig. 2b). Notably, while the CJYZ section contains only dolostones, the JLW section includes both dolostones and limestones.

One could argue that these mineralogical differences might contribute to some variations in Li isotopes. Indeed, studies of modern carbonate suggest that the mineralogy of marine carbonates strongly influences the $\Delta^7Li_{sw\text{-}carbonate}$, with $\Delta^7Li_{sw\text{-}aragonite} \approx 2.0‰$[34] and $\Delta^7Li_{sw\text{-}calcite} = 6.1 \pm 1.3‰$[35]. Limestones would exhibit lighter Li isotopic values by ~4‰ compared to their aragonite counterparts. Therefore, the observed Li isotopic excursions cannot be fully attributed to changes in mineral composition. Moreover, despite the differences in depositional thickness, mineralogy, and sedimentary sequences between the two sections, both profiles reproduce similar values and secular trends in Li isotope compositions, as well as elemental concentrations (such as Al/(Mg+Ca) and Mn/Sr). This suggests that the recorded variations most likely reflect genuine seawater changes rather than artifacts of mineralogical differences.

### Evaluations of diagenesis effect

All sedimentary rocks undergo diagenesis; the key question is whether diagenetic alteration has substantially modified the original Li isotopic signatures in the studied carbonates. Diagenesis can have complex impacts

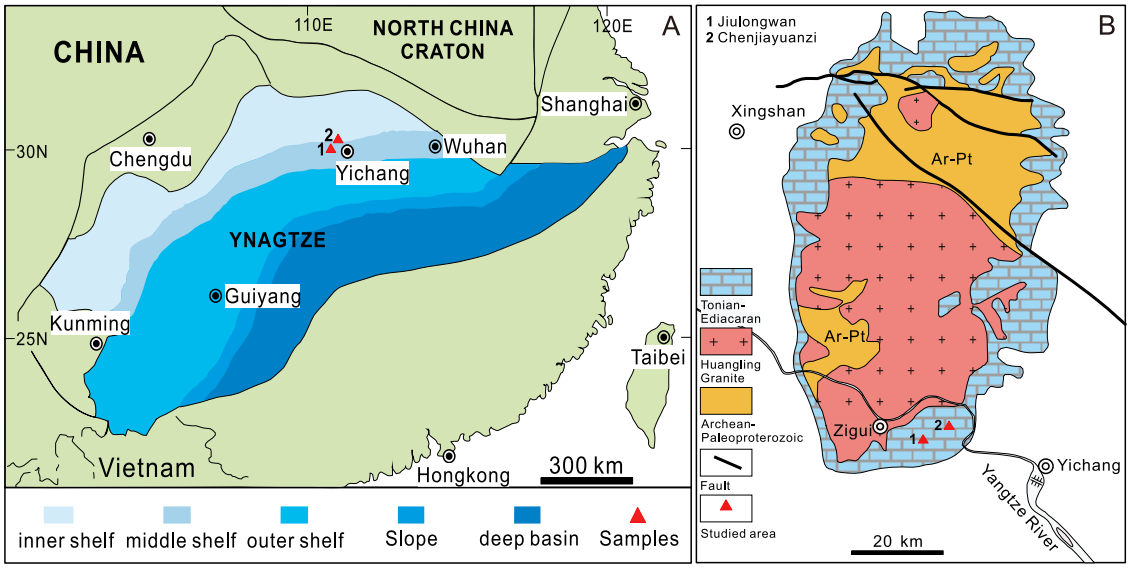


**Fig. 1 | Paleogeographic and geological maps of the Ediacaran Doushantuo Formation in South China. A** Paleogeographic reconstruction of the Ediacaran Yangtze platform[19,57]. Red triangles are the sample location. **B** Geological map of the Yangtze Gorges area, Hubei Province[30].

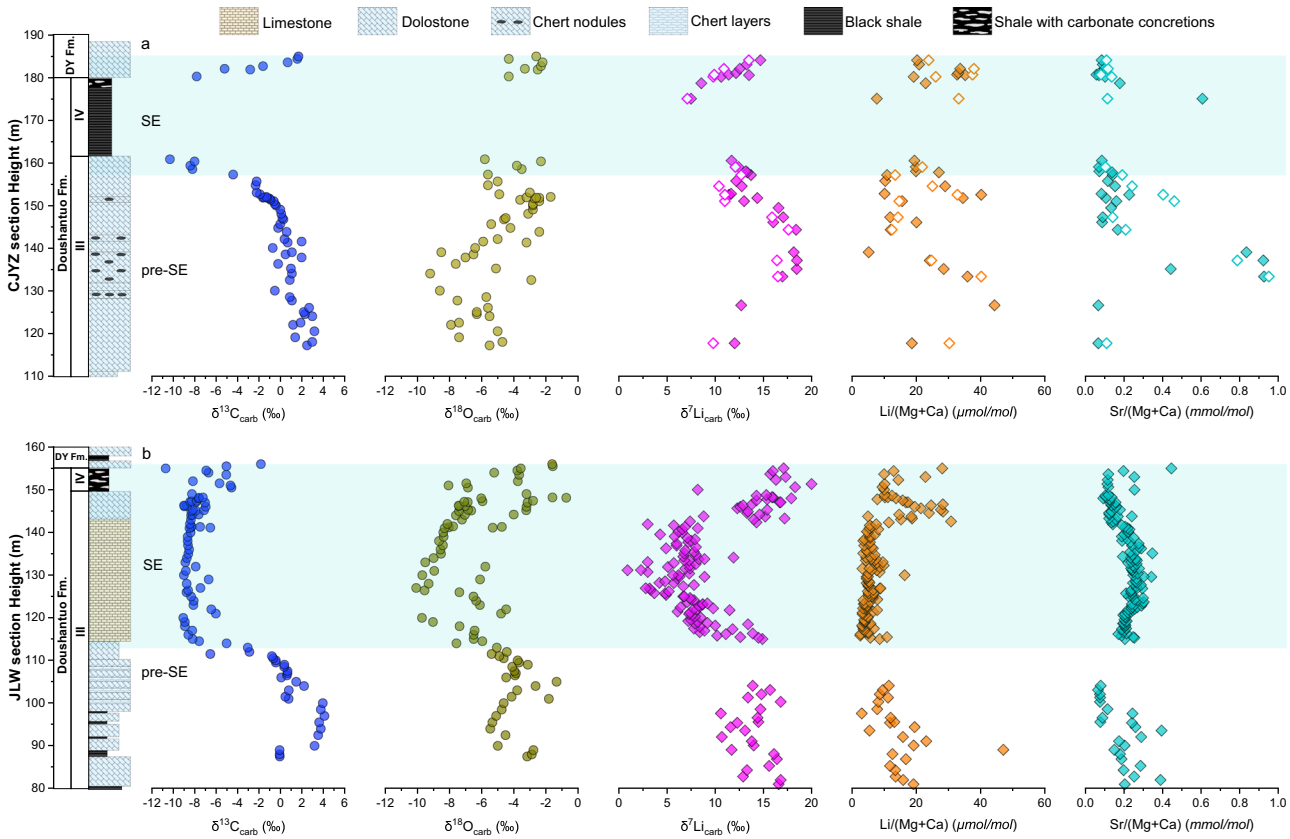


**Fig. 2 | Stratigraphic columns with isotopic and elemental profiles of CJYZ and JLW sections.** Stratigraphic column with $\delta^{13}C_{carb}$30,33, $\delta^{18}O_{carb}$30,33, $\delta^{7}Li_{carb,}$ and elemental profiles of the (**a**) CJYZ and **b** JLW sections. The Shuram Excursion event is marked by the light blue region. The filled and open diamonds in the CJYZ section represent bulk carbonate data that leached by 0.3 M and 0.5 M acetic acid, respectively. The JLW section has a short gap in the pre-SE due to poor outcrop during our collection of samples.

on the Li isotope composition of carbonates: rock-buffered diagenesis generally preserves the Li isotope composition of the precursor carbonate, whereas fluid-buffered diagenesis introduces variable Li isotope signatures depending on the characteristics of the reacting fluids[22]. Seawater-buffered diagenesis, for instance, would elevate $\delta^{7}$Li values in marine limestones and dolostones, causing them to approach the composition of ambient seawater[22,34]. Conversely, meteoric diagenetic carbonates, likely shaped by sediment-buffered conditions, tend to inherit the original $\delta^{7}$Li signatures of primary carbonates[34].

One possible scenario could involve seawater-buffered diagenesis for the pre-SE and end-SE intervals and meteoric alteration or sediment-buffered diagenesis during the SE, which might explain the observed

negative Li isotopic excursion during the SE. However, we consider this scenario highly unlikely for several reasons. First, recent in-situ carbon isotope studies have shown that the extremely negative $\delta^{13}C_{carb}$ observed are primary products of the Ediacaran surface environment rather than products of diagenesis[8,36]. Thus, the global presence of the SE and the coupled $\delta^{7}Li_{carb}$ and $\delta^{13}C_{carb}$ variations in both the CJYZ and JLW sections strongly suggest a primary seawater origin. Additionally, the SE has been proposed to coincide with a marine transgression event, which reduces the likelihood of carbonate sediments being exposed to meteoric alteration. On the contrary, transgression would increase the potential for seawater-buffered diagenesis during the SE[6]. Furthermore, a seawater-buffered diagenetic process in the pre-SE and the end of SE would be expected to yield significantly lower Sr/(Mg+Ca) ratios, higher Li/(Mg+Ca) ratios, and positive correlations in Li/(Mg+Ca) vs.$\delta^{7}Li_{carb}$[22,34], which is not observed in either section (Supplementary Fig. 1c).

A numerical mass-balance model of early marine carbonate diagenesis was used to quantify the influence of diagenesis on the Li isotopic compositions of the studied bulk carbonates[37,38]. This model forecasts diagnostic trajectories in cross-plots of $\delta^{7}$Li vs. Li/(Mg+Ca) and Sr/(Mg+Ca), illustrating the conditions from sediment-buffered to fluid-buffered diagenesis (Supplementary Fig. 3). During transgression, seawater flooding in shallow-water settings is suggested to primarily induce seawater-buffered diagenesis[6]. In locations closest to the fluid source (Box 1), fluid-buffered diagenetic alteration of aragonite to dolomite results in simultaneous shifts in Li/(Ca + Mg), Sr/(Ca+Mg), and $\delta^{7}$Li values. At the farthest point along the flow path (Box 100), sediment-buffered diagenesis leads to lower Sr/(Ca+Mg) and Li/(Ca+Mg) ratios and a more muted Li isotopic shift (Supplementary Fig. 3).

The best-fit scenario for the CJYZ samples suggests at least two phases of diagenetic alteration, although some data points fall outside the range of the diagenetic model. Modeling #1, applied to pre-SE samples, and Modeling #2, for SE and end-SE samples, indicate a decline in $\delta^{7}Li_{SW}$ from ~ +20‰ to SE levels of ~ +15‰ (or lower for the lack of data during the climax of the SE in this section). The JLW section can be best modeled by four stages of diagenetic alteration, suggesting a decrease of $\delta^{7}Li_{SW}$ from pre-SE (~ +20‰, red to orange dots in Modeling #3) to SE (the initial stage of SE ~ +15‰, Modeling #4; SE climax at ~+ 12‰, Modeling #5), followed by a return to ~ +20‰ at the end-SE (Modeling #3, blue dots). Although this diagenetic modeling does not capture the full complexity of natural processes, it nonetheless reveals a significant negative shift in seawater Li isotopes during the SE, even with extensive diagenetic alteration.

## Reconstructed seawater Li isotopes

Consider that our samples may be affected by seawater-buffered diagenetic process. Conservative fractionation factors of $\Delta^{7}Li_{sw\text{-}dolostones}$ ~ 2.0 ± 2‰ and $\Delta^{7}Li_{sw\text{-}limestones}$ ~ 6.1 ± 2‰ were used to calculate the seawater Li isotopic compositions[34,35]. Estimated $\delta^{7}Li_{sw}$ values agree well between the two sections, showing large excursions of > 5‰ in the CJYZ section (incomplete due to the absence of carbonate during black shale deposition) and ~5–10‰ in the JLW section during the SE. A baseline $\delta^{7}Li_{sw}$ of approximately +18 ± 3‰ is observed for pre- and the end of SE, dropping to around +6.9 to 15‰ during the SE. These SE values are significantly lighter than those of modern seawater, aligning with recent findings that suggest Precambrian seawater may have sustained lower $\delta^{7}Li_{sw}$ values, averaging around ~ 6–16‰[27].

Constraining the Li concentration and Li inventory of SE seawater from the Li/(Mg+Ca) ratios of the studied carbonates is challenging. Li partitioning between seawater and carbonates can be influenced by various factors, including temperature, pH, carbonate growth rate, and mineralogy[39,40]. Therefore, the observed lower Li/(Mg+Ca) ratios during the SE compared to pre-SE in these sections do not necessarily reflect a reduced Li inventory; instead, they may result from the factors such as higher temperatures, slower calcite growth rates, increased pH, or a shift in mineralogy from dolostone to limestone, with mineralogical change likely being the dominant factor. The CJYZ section, composed exclusively of dolostones, does not show this Li/(Mg+Ca) shift into the SE, suggesting that the observed low Li/(Mg+Ca) ratios in the JLW section are likely due to mineralogical differences.

Secular variations in seawater strontium concentration can be inferred from bulk carbonate sediments when mineralogical and diagenetic effects are accounted for[41]. Since aragonite has a significantly higher Sr distribution coefficient than calcite ($D_{Sr\ arag} \approx 1$ versus $D_{Sr\ calc} \approx 0.1$)[41], the higher Sr/(Mg+Ca) ratios observed in pre-SE and end-SE dolostones likely reflect the signatures of precursor aragonites. The change in Sr/(Mg+Ca) ratios during the SE, which consists mostly of limestones in the JLW section, cannot be explained solely by mineralogical or diagenetic effects. Instead, this shift aligns with the secular Sr isotope trend, suggesting a change in seawater Sr inventory during the SE (Fig. 3b).

In summary, SE seawater was characterized by a negative Li isotope excursion and a positive Sr isotope excursion (with a possibly elevated Sr inventory), both of which closely correlate with $\delta^{13}C_{carb}$ in the samples studied[30,33].

## Restrict or open ocean?

Determining whether the reconstructed seawater Li isotope values represent a restricted environment or open ocean waters is crucial for interpreting the data. In the modern ocean, lithium has a short mixing time (~1000 years), which is much less than the residence time of Li in seawater (~1 million years)[24]. Consequently, seawater Li isotopic composition remains homogeneous both horizontally and vertically, even in semi-restricted seas like the Mediterranean[42]. Furthermore, seawater has significantly higher Li concentrations (~25.7 μM) than freshwater (~0.2 μM), leading to dominant seawater Li isotopic signatures in shelf and gulf environments and even influencing estuarine river waters in delta regions[43]. The JLW and CJYZ sections were likely deposited in an inner-shelf environment[30,33]. Numerous geochemical proxies—including C, O, S, Ca, and Mg isotopes, as well as carbonate-associated phosphate concentrations—show strong correlations between the JLW section and global SE sections[5,6,13,18,33,36]. These observations suggest that the Li isotopic signatures in the studied sections likely reflect global open ocean water.

## Modeling Li-Sr system changes during the SE

The Li isotope records, combined with the seawater Sr isotope secular trend and geochronological constraints on the SE[3], provide a foundation for quantitatively constraining Li and Sr geochemical dynamics. Possible scenarios explaining Earth system changes during the SE were explored using our newly developed dynamic box model (see method and Supplementary Note 4 for model details). The model is driven by factors such as tectonic uplift (U), seafloor spreading rate (R), the exposed areas of basalt (Abas) and granite (Agran), weathering intensity (WI), and temperature (T). The modeling period spans from 585 Ma to 555 Ma, covering three stages: pre-SE (585–574 Ma), the SE (~574–567.3 Ma), and post-SE (~567.3–555 Ma). Background parameters were adopted from present-day values and adjusted to align with the geological and geochemical records of the Ediacaran period (Supplementary Tables 2–3). We tested each scenario individually to determine whether it captured one or more main characteristics of the SE and then combined these with geological constraints to evaluate the best-fit scenario.

Increased seafloor spreading (Scenario 1a) results in a marked decline in seawater Sr isotopes, an increase in Sr inventory, and a mild decrease in Li isotopes, which contrasts with the observed data. A scenario with reduced spreading (Supplementary Fig. 6), while compatible with the Sr isotope increase during the SE, predicts a low Sr inventory and slightly elevated Li isotope compositions, which diverge from observed data. Increased tectonic uplift (Scenario 2) aligns with seawater Sr and Li isotope trends if the weathering regime shifts from incongruent in the pre-SE to congruent in the SE (Supplementary Fig. 7). However, this would require an unrealistic increase in tectonic uplift (~2.3 times pre-SE levels) to produce the Sr and Li isotope shifts and would also necessitate highly congruent weathering

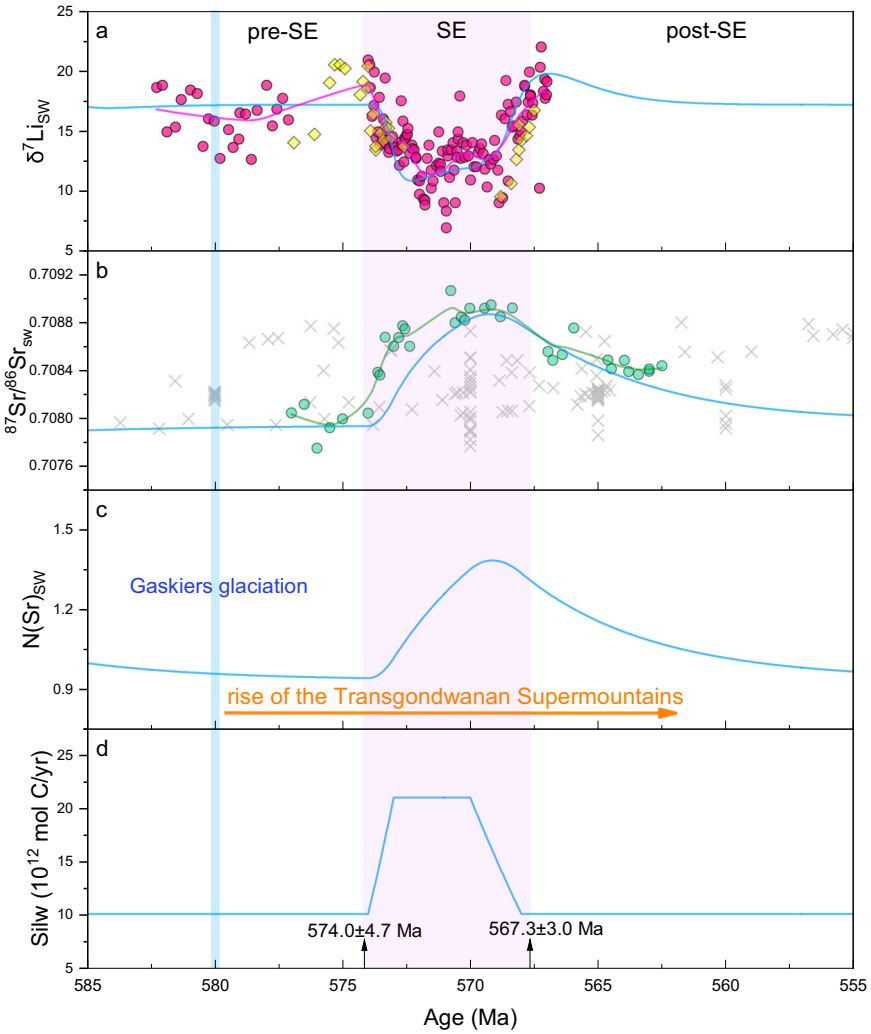


**Fig. 3 | Modeling results (scenario 7) that best replicate the observed Li and Sr isotope perturbations across the SE event.** For detailed driven parameters please see the Supplementary Table. 3. Time and duration of the Gaskiers (~ 580 Ma, cyan band)[45], the rise of the Transgondwanan Supermountains (~580−550 Ma, yellow arrow)[48], and the Shuram excursion (~574−567.3 Ma, light pink region)[3] are also shown. **a** Modeled $\delta^7Li_{SW}$ (blue line) matches the observed seawater Li isotope variations (pink dots are the JLW samples; yellow diamonds are CJYZ samples; pink line is the smoothing spline fits of the data) during the SE. **b** Modeled seawater $^{87}Sr/^{86}Sr$ (blue line) mimic compilation values (gray crosses[31]) and high-resolution radiogenic Sr isotope excursion (green dots and the green line is the smoothing spline fits) in the Doushantuo Formation[21]. **c** Modeled seawater Sr inventory ($N_{Sr}$) shows a first increase and subsequently decline trend. **d** The modeled silicate weathering rate shows pulsed rises from baseline values of $10.5 \times 10^{12}$ mol C/yr to ~$20 \times 10^{12}$ mol C/yr in the SE event, largely due to the abrupt increase in uplift (U) and temperature (T) during the SE in the model.

conditions throughout the SE. Increased tectonic uplift would further reduce $pCO_2$, leading to global cooling, likely causing a sea-level drop and higher Li/(Ca+Mg) ratios in carbonates.

A scenario with a larger global exposed granite area (Scenario 3) or a pulsed injection of $CO_2$ into the atmosphere (Scenario 4) approximates the Sr isotope data but has minimal effect on $\delta^7Li$ (Supplementary Figs. 8–9). Scenario 4 would also require an unrealistically high $pCO_2$ (~62 times present-day levels) to match the Sr isotope trend. In contrast, seawater $\delta^7Li$ is highly sensitive to changes in chemical weathering intensity (scenario 5), while Sr isotopes remain largely unaffected (Supplementary Fig. 10). Thus, no single process reproduces the observed trends in Li and Sr isotopes. Combining Scenarios 4 and 5 (Scenario 6) fits well with the Li and Sr isotope data (Supplementary Fig. 11), though it contradicts the modern observation that higher temperatures are usually accompanied by increased weathering intensity.

Finally, by combining elements of Scenarios 2, 4, and 5, we modeled an increase in tectonic uplift concurrent with a moderate $CO_2$ injection at the onset of the SE, followed by a decline in chemical weathering intensity and continued $CO_2$ consumption via enhanced weathering (Scenario 7). This combination best captures the key aspects of the SE (Fig. 3). Therefore, based on available geological constraints, we selected Scenario 7 for further discussion.

### Enhanced congruent continental weathering during the SE

Our modeling results indicate that multiple geological processes must be integrated to match the observed secular change in Li and Sr isotopes across the SE. The coupled variations in $\delta^7Li_{carb}$ and $\delta^{13}C_{carb}$ in the investigated samples should thus be interpreted in a global, coherent context.

In the Shuram Formation, Oman, the SE spans hundreds of meters of stratigraphic thickness, with an estimated duration of at least 7 million years[2,3,6]. To simulate the seawater $\delta^7Li$ and $^{87}Sr/^{86}Sr$ perturbations during the SE, a pulse of enhanced continental weathering lasting ~7 Myr is required (Fig. 3). Our dynamic box model (Scenario 7) suggests a pulsed increase in tectonic uplift (to ~1.3 times the modern level) concurrent with a moderate $CO_2$ injection at the SE onset. This increase likely led to a rapid rise in global surface temperatures (~1.5 °C) and an accelerated hydrological cycle[44]. Elevated tectonic uplift would have exposed fresh minerals for weathering, fostering high erosion rates and enhanced, near-congruent chemical weathering. As $CO_2$ was subsequently consumed by enhanced weathering, $pCO_2$ and temperature would gradually decrease, leading to a slowdown in weathering rates and a return to pre-SE weathering conditions.

A pulsed increase in riverine input during the SE, with $F_{riv}$ rising to ~ $12 \times 10^{10}$ mole/yr and $\delta^7Li_{riv}$ decreasing to +7‰, aligns well with observed seawater $\delta^7Li$ trends (Fig. 3a). This riverine boost likely stemmed from increased riverine dissolved [Li] as the weathering regime shifted from incongruent to congruent. Concurrently, the continental weathering rate (*Silw*) increased to ~ $20 \times 10^{12}$ mol C/yr during the SE, about 1.6 times the modern value (Fig. 3d), driven by higher uplift and temperatures in the model. Such conditions suggest a nutrient surplus during this interval. Calculations show a relatively short Li residence time ($\tau_{Li}$ = $Inventory_{Li}$ / $Flux_{Li}$) of 0.3–0.5 Myr at the SE onset due to high Li fluxes, enabling rapid $\delta^7Li_{SW}$ changes, which extended to ~1.1 Myr as the seawater Li inventory reached its maximum. This modeling closely matches observed data, with

an initial drop in $\delta^7Li_{SW}$ from ~ +18‰ to and then maintained at low values (~ +13‰) for ~ 3-4 Myr at ~ 573–569 Ma, followed by a rapid rise to ~+19‰ at the end of SE (Fig. 3a).

The long-term seawater Sr isotopic trend, together with Sr isotope data from local carbonate successions, constrains the Sr isotope modeling. During the SE, seawater $^{87}Sr/^{86}Sr$ values increase from 0.7081 to 0.7089 and then retreat to ~0.7085 (Fig. 3b)[21]. In model Scenario 7, pulsed uplift and temperature increase effectively replicate the seawater $^{87}Sr/^{86}Sr$ and Sr inventory changes, matching published data, and aligning with Li isotope modeling to support pulsed enhanced continental weathering during the SE. Unlike $\delta^7Li_{SW}$, a prolonged decline in $^{87}Sr/^{86}Sr$ in the aftermath of the SE is observed (Fig. 3a, b), likely due to the large Sr inventory and, consequently, a longer Sr residence time in SE oceans.

While pulsed enhanced continental weathering aligns well with observed data, the precise geological driver for this weathering pulse remains somewhat uncertain. The Gaskiers glaciation (~ 580 Ma), which predates the SE with a relatively short duration of ~340 kyr, appears an unlikely candidate[45]. Increased $CO_2$ degassing following the opening of the Iapetus Ocean after ~615 Ma may have facilitated continental weathering, but its mild impact on weathering and timing does not fully align with SE dynamics[46]. The rise and growth of the 8000-km-long, >1000-km-wide Transgondwanan Supermountains, formed during the India-Africa collision between ~580–550 Ma[47], likely fostered favorable conditions for congruent weathering with high denudation rates[48]. Concurrently, the collision of the Amazon and Rio de la Plata Cratons in South America with the Congo-Tanzanian and Kalahari Cratons in Africa (~590–550 Ma) gave rise to the 4000-km-long, 400-km-wide Adamastor Orogen[49]. The presence of the oldest lawsonite-bearing blueschists and eclogites confirms significant crustal thickening between ~580 and 550 Ma, broadly overlapping the SE[2,6,48]. Higher erosion rates associated with these orogens likely increased sedimentation rates, supporting congruent weathering and a pulse of high $F_{riv}$ with low $\delta^7Li_{riv}$ lasting ~7 Myr[50].

Active collisional orogens are also significant global $CO_2$ sources[51] and $CO_2$ injection into the atmosphere from both magmatic and metamorphic processes likely coincided with tectonic uplift. A pulse of mantle-derived $CO_2$ from carbonatite-alkaline magmatism may have occurred during the SE, as supported by a pronounced peak in cumulative U–Pb age data for carbonatite-alkaline detrital zircons at ~576 Ma[52]. Although precise constraints on pre-Cambrian volcanic $CO_2$ emissions are limited, rapid increases in atmospheric $CO_2$ concentration (up to ~1300 ppm) in the Late Ediacaran have been suggested in connection with the SE event[53]. This would have initiated a warm period, accelerating the hydrological cycle and likely causing a sea-level rise consistent with SE marine transgression events[6]. As $CO_2$ and freshly exposed minerals were subsequently consumed by enhanced weathering, $pCO_2$ and temperatures likely declined, leading to a stabilization of weathering rates and a return to pre-SE conditions by the SE's end.

### Driving mechanisms of SE and oceanic oxygenation

Although there is ongoing debate regarding whether the SE coincided with oceanic oxygenation[11,12], many geochemical studies suggest that the SE may represent Earth's first documented widespread deep-ocean oxidation event[13–16,18–20,54]. A growing body of evidence suggests that marine oxygenation during the SE was transient, with the deep ocean only partially oxidized, indicating the widespread coexistence of oxic and anoxic zones across the seafloor[3,19,55]. Furthermore, there remains debate over whether atmospheric and oceanic oxygenation were coupled during the SE[19,54].

Numerical modeling indicates that atmospheric oxygen levels increased monotonically from ~630 Ma to ~590 Ma, stabilizing at ~0.6 PAL for the remainder of the Ediacaran, whereas deep-ocean oxygenation occurred only transiently during the SE[54]. In contrast, organic geochemical proxies (e.g., pristane/phytane ratios) reveal two distinct phases of marine oxygenation in the Ediacaran, first at 630–600 Ma and again during the SE, with these proxies exhibiting a negative correlation with carbon isotopes, supporting the hypothesis of coupled atmospheric-deep ocean oxygenation during the SE[19].

In a world with an oxygenated atmosphere but an anoxic ocean, a massive sulfate ($SO_4^{2-}$) influx at the onset of the SE may have served as a direct electron acceptor for DOC oxidation, releasing organically bound $CO_2$ and P. This process would have elevated oceanic P levels and atmospheric $pCO_2$, further enhancing P input via silicate weathering. This interpretation is supported by SE carbonate P records, which document two pulsed increases in marine P concentrations during the falling and rising limbs of the SE[20]. A five-stage model has been proposed to explain these P fluctuations, incorporating positive feedback from large-scale DOC oxidation on P availability and negative feedback from ocean anoxia on P burial[20]. Alternative mechanisms, such as sustained water-column ventilation and atmospheric $O_2$-driven sulfur oxidation during the SE, have also been suggested[13]. However, regardless of whether atmospheric and oceanic oxygenation were coupled, all these mechanisms require an external trigger to initiate sulfate delivery or water-column ventilation.

Pulse-enhanced continental weathering may represent the most plausible external driver for SE oceanic oxygenation. Initially, it would increase the flux of terrestrial nutrients into the ocean, with potential additional contributions from intensified evaporite or pyrite oxidative weathering (supplying sulfate to the ocean). The rise in P availability would have directly stimulated shallow-marine primary productivity, while concurrent sulfate input could have oxidized the DOC reservoir, liberating organically bound P and $CO_2$, thereby initiating positive feedback on marine productivity and continental weathering. The high organic carbon burial rates during the SE, as evidenced by the widespread occurrence of Ediacaran black shales and organic-rich mudstones in Oman, China, northwestern Canada, East Greenland, Svalbard, central Australia, North Africa, India, Pakistan, and Siberia, support pulsed increases in marine primary productivity[48]. Additionally, elevated temperatures and an intensified hydrological cycle during the SE may have strengthened oceanic circulation, enhancing water-column ventilation (Fig. 4).

The initial decoupling and subsequent covariation of $\delta^{13}C_{org}$ and $\delta^{13}C_{carb}$ during the SE succession suggest the presence of a large, ultimately oxidized DOC reservoir in the Ediacaran Ocean[9]. Oxidation of upwelling DOC may have triggered the negative carbon isotope excursion observed during the SE. This process likely occurred most frequently in slope regions where oxygenated waters interacted with DOC upwelling, whereas in shallow-water settings, particularly in restricted basins, DOC upwelling was limited or absent (Fig. 4). This model aligns with observations that Shuram carbon isotope excursions are most pronounced in slope environments but diminish or disappear in shallow-water settings[6]. Nevertheless, key uncertainties persist, particularly regarding whether sulfate or $O_2$ (derived from algal photosynthesis or ventilation-introduced atmospheric oxygen) served as the primary electron acceptor for DOC oxidation.

Ventilation-driven oxidation[13] not only lacks a clear external trigger but also fails to constrain the termination process of the SE. At the SE onset, the deep ocean was oxygen-poor but may have received a substantial sulfate influx via enhanced evaporite weathering[54]. A "sulfate-driven" DOC oxidation mechanism could operate more rapidly and at greater depths than P-driven photosynthetic $O_2$ production, which would primarily oxidize DOC at oxic-anoxic interfaces via upwelling. In either scenario, DOC reservoir oxygenation may have persisted until its depletion or until continental weathering weakened due to negative feedback effects, reducing nutrient inputs and allowing primary productivity to recover to pre-SE levels.

Based on coupled variations in $\delta^7Li_{carb}$, $^{87}Sr/^{86}Sr$, and $\delta^{13}C_{carb}$, we propose that pulse-enhanced continental weathering likely served as the primary trigger for seawater oxidation and played a central role in shaping climate, marine chemistry, and Earth's surface oxidation state during the SE. Increased nutrient availability, coupled with a transient rise in $O_2$ confined to shallow continental shelves, may have created favorable conditions for the

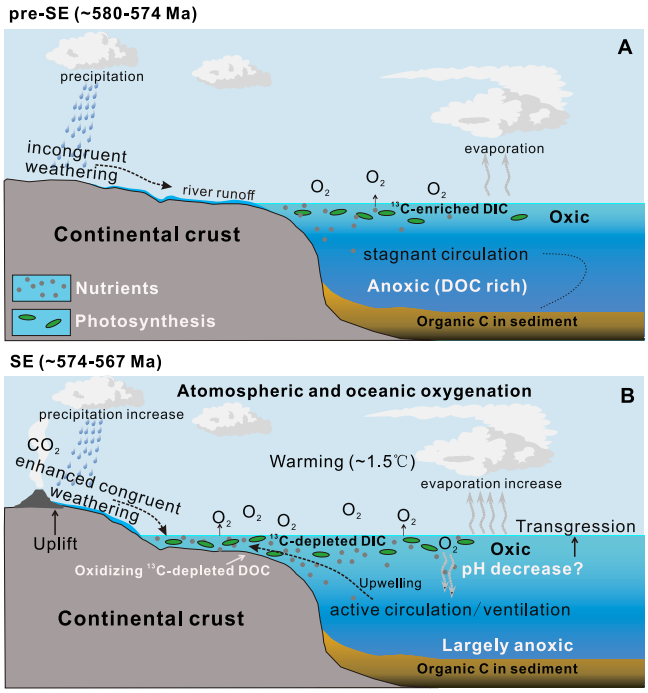


**Fig. 4 | Schematic presentation of the climate-ocean redox change before (~580–574 Ma) and during (~574–567 Ma) the Shuram Excursion.**
**A** Incongruent weathering and limited nutrient supply in an anoxic pre-SE world. **B** The rise of the Transgondwanan Supermountains caused continental uplift and injection of $CO_2$ into the atmosphere, leading to global warming, accelerated hydrological cycle, possible sea-level rise, and enhanced, near-congruent continental weathering during the SE. Enhanced continental weathering profoundly increases the nutrient inputs to the ocean and boosts primary production, leading to an oxygenation event and possibly the negative $\delta^{13}C_{carb}$ excursion by oxidizing the dissolved organic carbon reservoir on the continental shelf. DOC: dissolved organic carbon. DIC: dissolved inorganic carbon.

evolution and proliferation of oxygen-utilizing "Ediacaran biota" in the late Ediacaran[56].

## Conclusions

High-precision Li isotope measurements from marine carbonates in the Chenjiayuanzi and Jiulongwan sections reveal pronounced declines in Li isotopes during the Ediacaran Shuram Carbon Isotope Excursion, coinciding with elevated seawater $^{87}Sr/^{86}Sr$ values. Evaluations of potential clay contamination, mineralogical effects, and diagenetic alterations suggest that the observed Li isotope trends likely reflect a primary feature of SE ocean conditions. Geochemical modeling indicates that pulsed, enhanced continental weathering occurred during the SE, potentially driven by the uplift of the Transgondwanan Supermountains and Adamastor Orogen. This may have led to a pulsed increase in tectonic uplift (to ~1.3 times modern levels) coupled with a moderate $CO_2$ injection into the atmosphere at the onset of the SE. Elevated tectonic uplift would have exposed fresh primary minerals, fueling weathering. Together with a rapid increase in global surface temperatures (~1.5 °C) and an accelerated hydrological cycle, these likely created conditions conducive to high erosion rates and enhanced, near-congruent chemical weathering (Fig. 4).

As $CO_2$ and freshly exposed minerals were progressively consumed by this intensified weathering, $pCO_2$ and temperature would eventually decrease, leading to a slowdown in the weathering rate and a return to the pre-SE weathering regime. Such pulsed continental weathering during the SE likely increased nutrient influx to the oceans, boosting primary production and potentially triggering an oxygenation event. This oxygenation may have contributed to the observed negative $\delta^{13}C_{carb}$ excursion by oxidizing upwelling DOC (Fig. 4). Though transient, this Late Ediacaran oxygenation event may have stimulated the evolution and proliferation of large oxygen-utilizing Ediacaran biota on shallow continental shelves.

Our findings provide direct geochemical evidence for pulse-enhanced continental weathering during the SE, suggesting it played a key role in regulating climate, seawater chemistry, and Earth's surface oxidation state in the SE world. Additionally, high $CO_2$ levels in the early SE may have led to decreased seawater pH, a hypothesis that could be further tested through boron isotope analyses.

## Methods

### Sampling

The Three Gorges area in South China preserves several well-exposed sections of Ediacaran-age strata, which include the Doushantuo and Dengying formations. The Doushantuo Formation is widely distributed across South China and was deposited in shelf marine environments along a passive continental margin[57]. It is subdivided into four lithostratigraphic members (I – IV). The SE (referred to as DOUNCE/EN3 in the Yangtze Gorges area) begins at the Member II/III boundary and ends at the base of the Dengying formation.

Samples for this study were collected from the Chenjiayuanzi (CJYZ) and Jiulongwan (JLW) sections, both of which correspond to the SE in the Yangtze Gorges area (South China) (Fig.1). These newly collected samples come from the same locations as those in previous studies[30,33], allowing alignment of C and O isotopic trends with our Li isotope data, though not on a one-to-one basis.

The CJYZ section is 180 m thick and lies directly above the Nantuo glacial diamictite. From bottom to top, it consists of a 2 m-thick cap carbonate (Member I); a 103 m-thick black shale with intercalations of thin to thick dolostone beds containing chert nodules (Member II); a 55 m-thick, light gray, medium- to thick-bedded dolostone with thin muddy dolostone layers, and the upper portion containing abundant 10–50 cm thick black chert bands, nodules, and silicified oolitic dolostone (Member III); and a 20-m-thick black shale with lenticular dolostone layers (Member IV)[30].

The JLW section, located ~10 km southeast of CJYZ, features a similar profile. It consists of a 5 m-thick cap dolostone (Member I); a 70 m-thick sequence of organic-rich shale and dolostone beds with abundant pea-sized chert nodules (Member II); a 70 m-thick dolostone with bedded chert in the lower part and limestone-dolostone "ribbon rocks" in the upper part (Member III); and a 10 m-thick organic-rich shale unit that is widespread across the Yangtze Gorges area (Member IV)[33].

A total of 179 fresh carbonate samples (30 from CJYZ and 149 from JLW) were selected from Doushantuo Members III, IV, and the base of the Dengying Formation (DY Fm.) for Li isotopic analysis. Due to poor outcrop conditions, there is a short gap in the samples from the JLW section prior to the SE. The samples were broken into small pieces in a sample crushing laboratory, handpicked to avoid fractures, veins, or weathering, and then powdered to 200 mesh for Li isotope and elemental analysis.

### Lithium isotope and elemental analysis

A chemical leaching method using dilute acetic acid was applied to analyze the Li isotopic composition of the carbonate fraction in dolostone and limestones. In this study, we conducted two batches of analyses on the CJYZ samples, using 0.3 M and 0.5 M acetic acid, respectively, to verify the robustness of the analytical procedure. Each sample underwent cleaning, leaching with dilute acetic acid, and purification of Li using an organic solvent-free liquid chromatography method. After adjusting to a targeted concentration (10 or 50 ng/g), Li isotopes were measured on two Neptune Plus MC-ICP-MS instruments at the University of Science and Technology of China and Hefei University of Technology.

Each measurement was bracketed before and after by a L-SVEC standard. The in-run precision for $^{7}Li/^{6}Li$ measurements was ≤ 0.2‰ for one block of 40 ratios. External precision, based on long-term monitoring of two in-house standards, $Li_{QC} = +8.8 \pm 0.3$ ‰ (2 SD, 2 years, $n = 186$) and $Li_{USTC-L} = -19.3 \pm 0.2$ ‰ (2 SD, 2 years, $n = 64$), as well as analysis of

international rock reference materials, including BHVO-2 = +4.3 ± 0.4‰ (2 SD, $n = 8$), GSP-2 = -0.8 ± 0.2‰ (2 SD, $n = 29$), and AGV-1 = +5.9 ± 0.4‰ (2 SD, $n = 9$), demonstrated precision better than 0.5‰.

Elemental concentrations were measured at the Hefei University of Technology on an Agilent™ 7900 Q-ICP-M for each leached solution. Detailed methods for Li isotopic and elemental are provided in the Supplementary data Tables 4–5.

### Numerical model of diagenesis

We employed a 1D-advection reaction model to simulate the flow of diagenetic fluid, such as seawater, through permeable carbonate sediments[37,38]. The model assumes a homogeneous sediment composition and divides the flow path into a specified number of segments, each with a consistent volume (1 $m^3$) and porosity (0.5) (box 1 to N). The dissolution of the original sediment and the simultaneous formation of diagenetic minerals were simulated over time. Diagenetic trajectories (ranging from "fluid-buffered" to "sediment-buffered") were constrained using cross-plots of $\delta^7$Li vs. Li/(Mg+Ca) and Sr/(Mg+Ca). A detailed description of the model is provided in the Supplementary Data.

### Geochemical box modeling of Li-Sr cycles

Dynamic box modeling was applied to constrain seawater Sr-Li fluctuations. The model is based on previously published Sr and Li isotope box models and the COPSE reloaded mode[23,24,44,46], with revisions to the Sr-Li cycles and flux functions to better reflect the geological conditions of the Ediacaran period (see Supplementary Table. 7 for equation references). The driving forces include tectonic uplift (U), seafloor spreading rate (R), the exposed area of basalt ($A_{bas}$) and granite ($A_{gran}$), weathering intensity (WI), and temperature (T and $pCO_2$). Modeling parameters are detailed in Supplementary Tables 2–3. For a comprehensive description of the model, including differential equations, present-day reservoir sizes, and fluxes, please refer to the Supplementary Table. 7.

We ran the Sr-Li model forward in time from 585 Ma to 555 Ma using pre-established parameters for the driving factors (Supplementary Table 3). The model estimates seawater Sr and Li isotope trends, successfully reproducing key patterns, suggesting that the modeled processes provide a plausible representation of global biogeochemical cycles during the SE.

## Data availability

All data supporting the findings of this study are available within the paper and its Supplementary Information. Supplementary Tables 1–3 are provided in the Supplementary Information file, while Supplementary Tables 4–8 are included in the Supplementary Data 1 file. Supplementary Data 1 are publicly available at https://doi.org/10.6084/m9.figshare.29069771.

## Code availability

Code for diagenesis modeling (in Python) is posted on GitHub (https://github.com/yangty95/1D-advection-reaction-model.git).

Received: 10 January 2024; Accepted: 27 May 2025;
Published online: 05 June 2025

## References

1. Droser, M. L., Tarhan, L. G. & Gehling, J. G. The rise of animals in a changing environment: global ecological innovation in the late Ediacaran. *AREPS* **45**, 593–617 (2017).
2. Grotzinger, J. P., Fike, D. A. & Fischer, W. W. Enigmatic origin of the largest-known carbon isotope excursion in Earth's history. *Nat. Geosci.* **4**, 285–292 (2011).
3. Rooney, A. D. et al. Calibrating the coevolution of Ediacaran life and environment. *Proc. Natl. Acad. Sci. USA.* **117**, 16824–16830 (2020).
4. Liu, Y. et al. The largest negative carbon isotope excursions in Neoproterozoic carbonates caused by recycled carbonatite volcanic ash. *Sci. Bull.* **66**, 1925–1931 (2021).
5. Wei, G.-Y. et al. On the origin of Shuram carbon isotope excursion in South China and its implication for Ediacaran atmospheric oxygen levels. *PreR* **375**, 106673 (2022).
6. Busch, J. F. et al. Global and local drivers of the Ediacaran Shuram carbon isotope excursion. *Earth Planet. Sci. Lett.* **579**, 117368 (2022).
7. Derry, L. A. A burial diagenesis origin for the Ediacaran Shuram–Wonoka carbon isotope anomaly. *Earth Planet. Sci. Lett.* **294**, 152–162 (2010).
8. Husson, J. M. et al. Large isotopic variability at the micron-scale in 'Shuram' excursion carbonates from South Australia. *Earth Planet. Sci. Lett*. **538**, 116211 (2020).
9. Fike, D. A., Grotzinger, J. P., Pratt, L. M. & Summons, R. E. Oxidation of the Ediacaran ocean. *Nature* **444**, 744–747 (2006).
10. Zhang, F. et al. Global marine redox changes drove the rise and fall of the Ediacara biota. *Geobiology* **17**, 594–610 (2019).
11. Ostrander, C. M. et al. Widespread seafloor anoxia during generation of the Ediacaran Shuram carbon isotope excursion. *Geobiology* **21**, 556−570 (2023).
12. Ostrander, C. M. Mulling and nulling the coeval rise of Ediacaran oxygen and animals. *Earth Planet. Sci. Lett.* **614**, 118187 (2023).
13. Wang, H. et al. Sulfate triple-oxygen-isotope evidence confirming oceanic oxygenation 570 million years ago. *Nat. Commun.* **14**, 4315 (2023).
14. Sahoo, S. K. et al. Oceanic oxygenation events in the anoxic Ediacaran ocean. *Geobiology* **14**, 457–468 (2016).
15. Mcfadden, K. A. et al. Pulsed oxidation and biological evolution in the Ediacaran Doushantuo formation. *Proc. Natl. Acad. Sci. USA.* **105**, 3197–3202 (2008).
16. Canfield, D. E. et al. Ferruginous conditions dominated later Neoproterozoic deep-water chemistry. *Science* **321**, 949–952 (2008).
17. Fan, H. et al. Constraining oceanic oxygenation during the Shuram excursion in South China using thallium isotopes. *Geobiology* **18**, 348–365 (2020).
18. Shi, W. et al. Sulfur isotope evidence for transient marine-shelf oxidation during the Ediacaran Shuram excursion. *Geology* **46**, 267–270 (2018).
19. Kaiho, K. et al. Oxygen increase and the pacing of early animal evolution. *GPC* **233**, 104364 (2024).
20. Dodd, M. S. et al. Uncovering the Ediacaran phosphorus cycle. *Nature* **618**, 974–980 (2023).
21. Sawaki, Y. et al. The Ediacaran radiogenic Sr isotope excursion in the Doushantuo formation in the three Gorges area, South China. *PreR* **176**, 46–64 (2010).
22. Dellinger, M. et al. The effects of diagenesis on lithium isotope ratios of shallow marine carbonates. *AmJS* **320**, 150–184 (2020).
23. Sun, H. et al. Rapid enhancement of chemical weathering recorded by extremely light seawater lithium isotopes at the Permian–Triassic boundary. *Proc. Natl. Acad. Sci. USA.* **115**, 3782–3787 (2018).
24. Misra, S. & Froelich, P. N. Lithium isotope history of Cenozoic seawater: changes in silicate weathering and reverse weathering. *Science* **335**, 818–823 (2012).
25. Dellinger, M. et al. Riverine Li isotope fractionation in the Amazon River basin controlled by the weathering regimes. *Geochim. Cosmochim. Acta* **164**, 71–93 (2015).
26. Pogge von Strandmann, P. A. et al. Lithium isotope evidence for enhanced weathering and erosion during the Paleocene-Eocene thermal maximum. *Sci. Adv.* **7**, eabh4224 (2021).
27. Kalderon-Asael, B. et al. A lithium-isotope perspective on the evolution of carbon and silicon cycles. *Nature* **595**, 394–398 (2021).
28. Pogge von Strandmann, P. A., Jenkyns, H. C. & Woodfine, R. G. Lithium isotope evidence for enhanced weathering during Oceanic Anoxic Event 2. *Nat. Geosci.* **6**, 668–672 (2013).
29. Li, G. & West, A. J. Evolution of Cenozoic seawater lithium isotopes: coupling of global denudation regime and shifting seawater sinks. *Earth Planet. Sci. Lett.* **401**, 284–293 (2014).

30. Liu, P. et al. High-resolution biostratigraphic and chemostratigraphic data from the Chenjiayuanzi section of the Doushantuo Formation in the Yangtze Gorges area, South China: Implication for subdivision and global correlation of the Ediacaran system. *PreR* **249**, 199–214 (2014).
31. Chen, X., Zhou, Y. & Shields, G. A. Progress towards an improved Precambrian seawater 87Sr/86Sr curve. *Earth-Science Reviews* **224**, 103869 (2022).
32. Quinby-Hunt, M., Wilde, P., Orth, C. & Berry, W. in Metalliferous black shales and related ore deposits. *In Proceedings, 1989 United StatesWorking Group Meeting,International Geological CorrelationProgram Project 2 54* 1037 (US Geological Survey Circular, 1989).
33. Jiang, G., Kaufman, A. J., Christie-Blick, N., Zhang, S. & Wu, H. Carbon isotope variability across the Ediacaran Yangtze platform in South China: implications for a large surface-to-deep ocean δ13C gradient. *Earth Planet. Sci. Lett.* **261**, 303–320 (2007).
34. Wei, G.-Y. et al. A 13 million-year record of Li isotope compositions in island carbonates: constraints on bulk inorganic carbonate as a global seawater Li isotope archive. *Geochim. Cosmochim. Acta* **344**, 59–72 (2023).
35. Pogge von Strandmann, P. A. et al. Assessing bulk carbonates as archives for seawater Li isotope ratios. *Chem. Geol.* **530**, 119338 (2019).
36. Cui, H. et al. Deposition or diagenesis? Probing the Ediacaran Shuram excursion in South China by SIMS. *GPC* **206**, 103591 (2021).
37. Ahm, A.-S. C., Bjerrum, C. J., Blättler, C. L., Swart, P. K. & Higgins, J. A. Quantifying early marine diagenesis in shallow-water carbonate sediments. *Geochim. Cosmochim. Acta* **236**, 140–159 (2018).
38. Murphy, J. G., Ahm, A.-S. C., Swart, P. K. & Higgins, J. A. Reconstructing the lithium isotopic composition (δ7Li) of seawater from shallow marine carbonate sediments. *Geochim. Cosmochim. Acta* **337**, 140–154 (2022).
39. Marriott, C. S., Henderson, G. M., Crompton, R., Staubwasser, M. & Shaw, S. Effect of mineralogy, salinity, and temperature on Li/Ca and Li isotope composition of calcium carbonate. *Chem. Geol.* **212**, 5–15 (2004).
40. Füger, A. et al. Effect of growth rate and pH on Li isotope fractionation during its incorporation in calcite. *Geochim. Cosmochim. Acta* **323**, 276–290 (2022).
41. Zhang, S., Zhou, R. & DePaolo, D. J. The seawater Sr/Ca ratio in the past 50 Myr from bulk carbonate sediments corrected for diagenesis. *Earth Planet. Sci. Lett.* **530**, 115949 (2020).
42. Jeffcoate, A. B., Elliott, T., Thomas, A. & Bouman, C. Precise/small sample size determinations of lithium isotopic compositions of geological reference materials and modern seawater by MC-ICP-MS. *Geostandards Geoanal. Res.* **28**, 161–172 (2004).
43. Yang, C., Vigier, N., Lian, E., Lai, Z. & Yang, S. Decoupling of dissolved and particulate Li isotopes during estuarine processes. *Geochem. Perspect. Lett.* **19**, 40–44 (2021).
44. Lenton, T. M., Daines, S. J. & Mills, B. J. W. COPSE reloaded: An improved model of biogeochemical cycling over Phanerozoic time. *Earth Sci. Rev.* **178**, 1–28 (2018).
45. Pu, J. P. et al. Dodging snowballs: geochronology of the Gaskiers glaciation and the first appearance of the Ediacaran biota. *Geology* **44**, 955–958 (2016).
46. Williams, J. J., Mills, B. J. & Lenton, T. M. A tectonically driven Ediacaran oxygenation event. *Nat. Commun.* **10**, 1–10 (2019).
47. Squire, R. J., Campbell, I. H., Allen, C. M. & Wilson, C. J. Did the Transgondwanan supermountain trigger the explosive radiation of animals on Earth? *Earth Planet. Sci. Lett.* **250**, 116–133 (2006).
48. Campbell, I. H. & Squire, R. J. The mountains that triggered the late Neoproterozoic increase in oxygen: the second great oxidation event. *Geochim. Cosmochim. Acta* **74**, 4187–4206 (2010).
49. Cawood, P. A. & Buchan, C. Linking accretionary orogenesis with supercontinent assembly. *Earth Sci. Rev.* **82**, 217–256 (2007).
50. Maffre, P., Goddéris, Y., Vigier, N., Moquet, J.-S. & Carretier, S. Modelling the riverine δ7Li variability throughout the Amazon Basin. *Chem. Geol.* **532**, 119336 (2020).
51. Groppo, C., Rolfo, F. & Frezzotti, M. L. CO2 outgassing during collisional orogeny is facilitated by the generation of immiscible fluids. *Commun. Earth Environ.* **3**, 13 (2022).
52. Paulsen, T., Deering, C., Sliwinski, J., Bachmann, O. & Guillong, M. Evidence for a spike in mantle carbon outgassing during the Ediacaran period. *Nat. Geosci.* **10**, 930–934 (2017).
53. Mckenzie, N. R. et al. Continental arc volcanism as the principal driver of icehouse-greenhouse variability. *Science* **352**, 444 (2016).
54. Shi, W. et al. Decoupled oxygenation of the Ediacaran ocean and atmosphere during the rise of early animals. *Earth Planet. Sci. Lett.* **591**, 117619 (2022).
55. Sperling, E. A. et al. Statistical analysis of iron geochemical data suggests limited late Proterozoic oxygenation. *Nature* **523**, 451–454 (2015).
56. Li, C., Shi, W., Cheng, M., Jin, C. & Algeo, T. J. The redox structure of Ediacaran and early Cambrian oceans and its controls. *Sci. Bull.* **65**, 2141–2149 (2020).
57. Jiang, G., Shi, X., Zhang, S., Wang, Y. & Xiao, S. Stratigraphy and paleogeography of the Ediacaran Doushantuo Formation (ca. 635–551Ma) in South China. *Gondwana Res.* **19**, 831–849 (2011).

## Acknowledgements

This work was financially supported by the National Natural Science Foundation of China (42230304; 42073003; 42373001), the Strategic Priority Research Program (B) of the Chinese Academy of Sciences (XDB41000000), and the Fundamental Research Funds for the Central Universities (JZ2019HGTB0071). We thank Dr. Jack Geary Murphy for insightful discussions, Dr. Jian Huang for sample collections, and Dr. Jing Lei for help during Li isotope analysis. Thanks to Dr. Carolina Ortiz Guerrero, Prof. Yanyan Zhao and other anonymous reviewers for their insightful feedback and constructive suggestions, which greatly improved this work. No permissions were required for sample collections.

## Author contributions

Y.X. and H.S. designed the project. H.S. and Y.X. wrote the manuscript. H.S. and F.T. obtained the Li isotope data. Y.X., H.S., Y.W., Z.A., and P.L. collected the samples. H.-O.G., C.G., F.W., E.S., M.Z., and T.Y. contributed to the discussion of the results and editing of the manuscript.

## Competing interests

The authors declare no competing interests.

## Additional information

**Supplementary information** The online version contains supplementary material available at https://doi.org/10.1038/s43247-025-02420-z.

**Correspondence** and requests for materials should be addressed to He Sun or Yilin Xiao.

**Peer review information** *Communications Earth & Environment* thanks Yanyan Zhao and the other, anonymous, reviewer(s) for their contribution to the peer review of this work. Primary Handling Editor: Carolina Ortiz Guerrero. A peer review file is available.

**Reprints and permissions information** is available at http://www.nature.com/reprints

**Publisher's note** Springer Nature remains neutral with regard to jurisdictional claims in published maps and institutional affiliations.

**Open Access** This article is licensed under a Creative Commons Attribution 4.0 International License, which permits use, sharing, adaptation, distribution and reproduction in any medium or format, as long as you give appropriate credit to the original author(s) and the source, provide a link to the Creative Commons licence, and indicate if changes were made. The images or other third party material in this article are included in the article's Creative Commons licence, unless indicated otherwise in a credit line to the material. If material is not included in the article's Creative Commons licence and your intended use is not permitted by statutory regulation or exceeds the permitted use, you will need to obtain permission directly from the copyright holder. To view a copy of this licence, visit http://creativecommons.org/licenses/by/4.0/.

© The Author(s) 2025